

Locality and Error Mitigation of Quantum Circuits

Minh C. Tran,¹ Kunal Sharma,¹ and Kristan Temme¹

¹*IBM Quantum, IBM T.J. Watson Research Center, Yorktown Heights, NY 10598, USA*

(Dated: March 14, 2023)

In this work, we study and improve two leading error mitigation techniques, namely Probabilistic Error Cancellation (PEC) and Zero-Noise Extrapolation (ZNE), for estimating the expectation value of local observables. For PEC, we introduce a new estimator that takes into account the light cone of the unitary circuit with respect to a target local observable. Given a fixed error tolerance, the sampling overhead for the new estimator can be several orders of magnitude smaller than the standard PEC estimators. For ZNE, we also use light-cone arguments to establish an error bound that closely captures the behavior of the bias that remains after extrapolation.

I. INTRODUCTION

Noisy quantum computers are scaling beyond the point their classical counterparts can efficiently simulate. A central question is whether, without error correction, noisy quantum devices can provide practical advantages over classical methods [1]. Most near-term algorithms involve the estimation of the expectation value of an observable after a shallow-depth circuit [2] and, to achieve quantum advantages, this estimation should be more accurate than those produced by classical algorithms [3].

Besides algorithmic errors, experimental inaccuracies degrade the desired output expectation values. The primary goal of error mitigation is to mitigate this effect and produce a better estimation of the expectation value, at the expense of increased sampling overhead and classical post-processing. Based on this idea, numerous mitigation techniques, such as Probabilistic Error Cancellation (PEC) [3, 4], Zero-Noise Extrapolation (ZNE) [3], and application-specific mitigation strategies employing symmetries and post-selection techniques have been introduced and demonstrated in recent years [5–24]. These techniques exploit only the structure of the noisy circuits and are applicable regardless of the observables we would like to measure.

In this work, we analyze the performance of two leading error mitigation strategies, namely PEC and ZNE, and show that they can be drastically improved when specialized to local observables. For PEC, we introduce an efficient estimator for the expectation value of an observable that takes into account its “light cone” [25, 26], reducing the sampling overhead of PEC by several orders of magnitude. Additionally, our estimator does not require tailoring the experimental procedure to the observables and, thus, can be retroactively applied to improve estimates from past PEC experiments.

While PEC estimators are unbiased and sampling overhead is the primary bottleneck of PEC, the main challenge in ZNE is to constrain the bias that remains after applying the Richardson extrapolation [3]. Here, we prove a bound on the bias in ZNE using light-cone arguments, showing ZNE performs significantly better when applied to local observables. In particular, our bound increases with the number of gates inside the light cones and closely capture the correct behavior of the bias.

II. SETUP

We consider an ideal circuit consisting of d unitary channels $\mathcal{U} = \mathcal{U}_d \cdots \mathcal{U}_1$. Each unitary channel may be a single quantum gate or a layer consisting of multiple gates. Let $\tilde{\mathcal{U}} = \tilde{\mathcal{U}}_d \cdots \tilde{\mathcal{U}}_1$ be the corresponding noisy circuit, where each noisy channel $\tilde{\mathcal{U}}_i$ is the composition of the ideal channel \mathcal{U}_i with a noise channel \mathcal{N}_i :

$$\tilde{\mathcal{U}}_i = \mathcal{U}_i \mathcal{N}_i. \quad (1)$$

The noise channels \mathcal{N}_i can be assumed to be Pauli channels when the idealized gates \mathcal{U}_i are Clifford gates. Generalized noise channels can always be transformed into Pauli channels via Pauli twirling [27–32]. A key prerequisite in many state-of-the-art error mitigation techniques is the ability to learn the noise channels \mathcal{N}_i . Fully characterizing a Pauli channel on n qubits generally requires resources scaling exponentially with n , but it can often be made efficient by considering the structure of \mathcal{N}_i on a particular device. To learn \mathcal{N}_i , we make the assumption that it can be written in Pauli-Lindblad form: $\mathcal{N}_i = e^{\mathcal{L}_i}$, where the generator

$$\mathcal{L}_i(\rho) = \sum_{j=1}^J \lambda_{i,j} (P_{i,j} \rho P_{i,j}^\dagger - \rho) = \sum_{j=1}^J \mathcal{L}_{i,j}(\rho) \quad (2)$$

for some $J \in \mathbb{N}$, $\mathcal{L}_{i,j}(\rho) \equiv \lambda_{i,j} (P_{i,j} \rho P_{i,j}^\dagger - \rho)$, and $P_{i,j}$ are Pauli strings on n qubits. The task of learning a general Pauli-Lindblad channel \mathcal{N}_i reduces to learning possibly $\mathcal{O}(4^n)$ parameters $\lambda_{i,j}$. However, if \mathcal{U}_i is a constant-depth layer, it is reasonable to assume that only low-weight Pauli strings contribute to the generator \mathcal{L}_i . It is then sufficient to learn the corresponding polynomially many parameters. Throughout this paper, we write the error channels in this Pauli-Lindblad form and assume they can be efficiently learned. Other than that, we do not make any locality assumption about the noise model. So, for example, qubits that are not connected by \mathcal{U}_i can still have correlated Pauli noise.

We note that, since two Pauli strings either commute or anti-commute, the generators $\mathcal{L}_{i,j}$ in Eq. (2) mutually commute. The noise channel therefore factorizes into J channels: $\mathcal{N}_i = \prod_{j=1}^J \mathcal{N}_{i,j}$, where

$$\mathcal{N}_{i,j}(\rho) = e^{\mathcal{L}_{i,j}}(\rho) = (1 - p_{i,j})\rho + p_{i,j}P_{i,j}\rho P_{i,j}^\dagger, \quad (3)$$

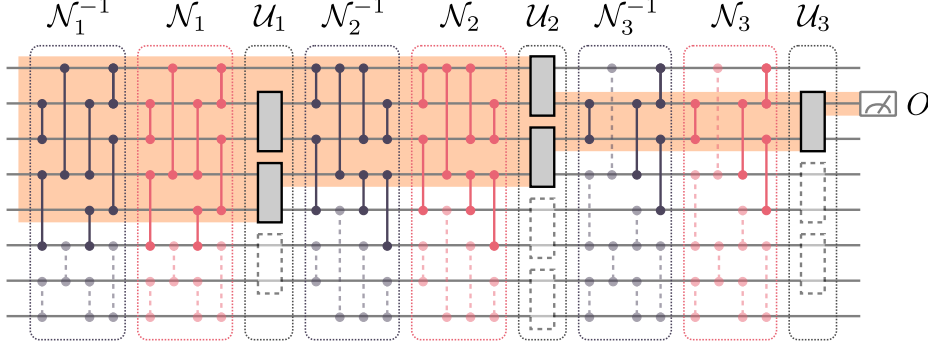


FIG. 1. An illustration of the light cone of the observable O initially supported on a single site. The ideal circuit $\mathcal{U}_3\mathcal{U}_2\mathcal{U}_1$ consists of three layers, each consists of gates (rectangular boxes) that may or may not act nontrivially on O (filled and empty boxes, respectively). The orange shaded area indicates the qubits inside the light cone μ_i defined in Eq. (11). The noisy version of the circuit consists of additional noise channels $\mathcal{N}_1, \mathcal{N}_2$, and \mathcal{N}_3 , which can be further decomposed into a series of Pauli channels in Eq. (3) (vertical lines). PEC cancels errors in the circuit by probabilistically applying the inverse $\mathcal{N}_{i,j}^{-1}$ at each layer. We reduce the sampling overhead of PEC by removing the contributions from error channels that lie outside the light cone (dashed vertical lines) in the construction of the local estimator [Eq. (12)].

and $p_{i,j} = (1 - e^{-2\lambda_{i,j}})/2 \in [0, 1/2)$ is the probability of the error $P_{i,j}$. Eq. (3) follows from the Taylor expansion of $\exp(\mathcal{L}_k)$ and the fact that $\mathcal{L}_k^2 = -2\mathcal{L}_k$. In terms of $\mathcal{N}_{i,j}$, the full noisy circuit is given by

$$\tilde{\mathcal{U}} = \prod_{i=1}^d \tilde{\mathcal{U}}_i = \prod_{i=1}^d \mathcal{U}_i \prod_{k=1}^J \mathcal{N}_{i,j}, \quad (4)$$

where $\prod_i \mathcal{A}_i = \cdots \mathcal{A}_2 \mathcal{A}_1$ is an ordered product.

Upon applying $\tilde{\mathcal{U}}$ on an initial state ρ , we measure in the computational basis $z \in \{0, 1\}^n$ to obtain m samples $\{z_1, \dots, z_m\}$. We use the samples to estimate the expectation value of an observable $O = \sum_z o_z |z\rangle\langle z|$: $\text{Tr}[\tilde{\mathcal{U}}(\rho)O] = \text{Tr}[\rho \tilde{\mathcal{U}}^\dagger(O)] \approx \frac{1}{m} \sum_{j=1}^m o_{z_j}$, where $\tilde{\mathcal{U}}^\dagger$ is the adjoint map of $\tilde{\mathcal{U}}$. We assume that $\|O\| = 1$, where $\|\cdot\|$ is the spectral norm, throughout this paper. Our main results apply to local observables—those supported on only a few sites, such as two-point correlators—and linear combinations of local observables.

III. PEC FOR LOCAL OBSERVABLES

The presence of noise deviates the expectation value of O from its ideal value. PEC mitigates this effect by additionally implementing the inverse of each noise channel:

$$\begin{aligned} \tilde{\mathcal{U}}_{\text{PEC}} &\equiv \prod_{i=1}^d \tilde{\mathcal{U}}_i \left(\prod_{j=1}^J \mathcal{N}_{i,j}^{-1} \right) \\ &= \prod_{i=1}^d \mathcal{U}_i \left(\prod_{k'=1}^J \mathcal{N}_{i,k'} \right) \left(\prod_{j=1}^J \mathcal{N}_{i,j}^{-1} \right) = \prod_{i=1}^d \mathcal{U}_i. \end{aligned} \quad (5)$$

Compared to the bare noisy circuit in Eq. (4), the addition of $\mathcal{N}_{i,j}^{-1}$ exactly negates $\mathcal{N}_{i,j}$ for all i, j , returning

the ideal circuit. One can exactly derive the inverse maps $\mathcal{N}_{i,j}^{-1}$ upon learning $\mathcal{N}_{i,j}$:

$$\mathcal{N}_{i,j}^{-1}(\rho) = \gamma_{i,j} \left[(1 - p_{i,j})\rho - p_{i,j} P_{i,j}^\dagger \rho P_{i,j} \right], \quad (6)$$

where $\gamma_{i,j} = e^{2\lambda_{i,j}} \geq 1$. To probabilistically implement $\mathcal{N}_{i,j}^{-1}(\rho)$, in each run of the circuit, we additionally apply $P_{i,j}$ before each $\tilde{\mathcal{U}}_i$ with probability $p_{i,j}$ and appropriately rescale the measurement results to account for the normalization factor $\gamma_{i,j}$. Explicitly, let $\sigma_{i,j} = \pm 1$ indicate whether $P_{i,j}$ was applied (-1) or not (1) and $\boldsymbol{\sigma} \in \{\pm 1\}^{dJ}$ be a vector containing all $\sigma_{i,j}$. Ref. [3] shows that

$$\hat{o}_z^{\text{PEC}}(\boldsymbol{\sigma}) = o_z(\boldsymbol{\sigma}) \prod_{i,j} \gamma_{i,j} \sigma_{i,j} \quad (7)$$

is an unbiased estimator for the ideal expectation value:

$$\mathbb{E}_{\boldsymbol{\sigma}} \mathbb{E}_z [\hat{o}_z^{\text{PEC}}(\boldsymbol{\sigma})] = \langle \mathcal{U}^\dagger(O) \rangle \quad (8)$$

where $\langle \cdot \rangle$ is the expectation value with respect to ρ . For readability, we may drop the implicit dependence on $\boldsymbol{\sigma}$ and simply write o_z and \hat{o}_z^{PEC} in the rest of the paper. Eq. (7) indicates that the variance of \hat{o}_z^{PEC} ,

$$\text{Var}[\hat{o}_z^{\text{PEC}}] = \mathcal{O} \left(\prod_{i,j} \gamma_{i,j}^2 \right) = \mathcal{O} \left(e^{4 \sum_{i,j} \lambda_{i,j}} \right), \quad (9)$$

is exponential in the total error rate $\lambda \equiv \sum_{i,j} \lambda_{i,j}$. For a generic depth- d circuit on n qubits, $\lambda = \mathcal{O}(nd)$, implying that the sampling overhead—the number of shots m it takes for \hat{o}_z^{PEC} to converge to the true value—grows exponentially both with the system size and with the depth of the circuit.

Given a local observable O , our first result is a construction of an efficient estimator o_z^{LoPEC} whose variance depends only on the “light cone” of \mathcal{U} with respect to O

and can be much smaller than that of \hat{o}_z^{PEC} . Our construction is based on an observation that the maps $\mathcal{N}_{i,j}$ and their inverse should not affect the expectation of O if they are supported entirely outside the light cone. Therefore, $p_{i,j}$ and the corresponding $\lambda_{i,j}$ should not contribute to the uncertainty in estimating $\langle O \rangle$.

For a concrete analysis, we first define the light cone of an observable O . We consider the Heisenberg picture, where an adjoint map $\tilde{\mathcal{U}}_{\text{PEC}}^\dagger$ is applied on O :

$$\tilde{\mathcal{U}}_{\text{PEC}}^\dagger = \prod_{i=d}^1 \left(\prod_{j=1}^J \mathcal{N}_{i,j}^{-1} \right) \tilde{\mathcal{U}}_i^\dagger. \quad (10)$$

We note that both $\mathcal{N}_{i,j}$ and their inverse are self-adjoint and mutually commute. In this picture, $\tilde{\mathcal{U}}_i^\dagger$ is the first channel to be applied on O . Let us assume that O is a local Pauli operator. Let $\text{supp}(O)$ denote the support of O and

$$\mu_i \supseteq \text{supp}(\mathcal{U}_i^\dagger \mathcal{U}_{i+1}^\dagger \cdots \mathcal{U}_d^\dagger(O)) \quad (11)$$

be a set of qubits that contains the support of O after evolving under the last ideal $d - i + 1$ unitary channels. We require that μ_i are efficiently classically computable for all i . There may be multiple choices of μ_i , but for the reasons we discuss below, it is ideal to pick the smallest sets that satisfy these requirements. The collection of μ_i for $i = 1, \dots, d$ forms what we call the light cone of O under \mathcal{U} . We say that a map $\mathcal{N}_{i,j}$ is outside the light cone if its support is distinct from μ_i , i.e. $\text{supp}(\mathcal{P}_{i,j}) \cap \mu_i = \emptyset$, and is inside otherwise. We note that Pauli channels $\mathcal{N}_{i,j}$ do not increase the support of O , allowing the light cone μ_i to be characterized entirely using the ideal circuit.

Let μ be the set of all (i, j) such that $\mathcal{N}_{i,j}$ are inside the light cone. We claim that

$$\hat{o}_z^{\text{LoPEC}}(\boldsymbol{\sigma}) \equiv o_z(\boldsymbol{\sigma}) \prod_{(i,j) \in \mu} \gamma_{i,j} \sigma_{i,j} \quad (12)$$

is also an unbiased estimator for the ideal expectation value:

$$\mathbb{E}_{\boldsymbol{\sigma}} \mathbb{E}_z[\hat{o}_z^{\text{LoPEC}}] = \langle \mathcal{U}^\dagger(O) \rangle. \quad (13)$$

We emphasize that o_z is the same outcomes after applying the standard PEC circuit in Eq. (5). But, the local PEC estimator \hat{o}_z^{LoPEC} has a simple, intuitive feature: its variance

$$\text{Var}[\hat{o}_z^{\text{LoPEC}}] = \mathcal{O} \left(e^{4 \sum_{(i,j) \in \mu} \lambda_{i,j}} \right) \quad (14)$$

only involves $\lambda_{i,j}$ that correspond to noise channels inside the light cone and may be much smaller than that of \hat{o}_z^{PEC} , as defined in Eq. (9).

We provide detail proof for our claims in Appendix A and illustrate its idea using a simple example. Consider an ideal circuit consisting of a single layer \mathcal{U} ($d = 1$) and a single Pauli noise channel \mathcal{N} ($J = 1$):

$$\mathcal{N}(\rho) = (1 - p)\rho + pP\rho P^\dagger, \quad (15)$$

where P is a Pauli string supported entirely outside the support of $\mathcal{U}^\dagger(O)$. The implementation of PEC would involve applying either $\tilde{\mathcal{U}} = \mathcal{U}\mathcal{N}$ with probability $1 - p$ or $\tilde{\mathcal{U}}\mathcal{P}$, where $\mathcal{P}(\rho) = P\rho P^\dagger$, with probability p . On average, the standard PEC estimator in Eq. (7) returns the ideal expectation value

$$\begin{aligned} & \gamma \left[(1 - p) \langle \tilde{\mathcal{U}}^\dagger(O) \rangle - p \langle \mathcal{P}\tilde{\mathcal{U}}^\dagger(O) \rangle \right] \\ & = \langle \mathcal{N}^{-1}\tilde{\mathcal{U}}^\dagger(O) \rangle = \langle \mathcal{U}^\dagger(O) \rangle, \end{aligned} \quad (16)$$

with a variance $\mathcal{O}(\gamma^2)$. In contrast, because \mathcal{N} is outside the light cone, the local estimator in Eq. (12) gives

$$(1 - p) \langle \tilde{\mathcal{U}}^\dagger(O) \rangle + p \langle \mathcal{P}\tilde{\mathcal{U}}^\dagger(O) \rangle = \langle \mathcal{N}\tilde{\mathcal{U}}^\dagger(O) \rangle \quad (17)$$

on average. Coupling with the fact that \mathcal{N} acts trivially on $\mathcal{U}^\dagger(O)$, we have $\langle \mathcal{N}\tilde{\mathcal{U}}^\dagger(O) \rangle = \langle \mathcal{N}^2\mathcal{U}^\dagger(O) \rangle = \langle \mathcal{U}^\dagger(O) \rangle$, which is also the ideal expectation value. However, the variance of this local estimator is $\mathcal{O}(1)$ instead of $\mathcal{O}(\gamma^2)$. Generalizing this argument to $d, J \geq 1$ proves our claim in Eq. (14).

To demonstrate the performance of the local PEC estimator, we numerically simulate the expectation value of a local observable after a noisy depth- d circuit on n qubits. The n qubits are arranged on a two-dimensional heavy hex lattice. Each layer of the circuit contains approximately $n/2$ CNOTs between distinct pairs of nearest-neighbor qubits. At each layer, we generate $J = 10n$ random noise channels such that the error rate per CNOT is approximately 4×10^{-3} . See Appendix C for the exact specifications of the random noisy circuit.

In Fig. 2(a), we plot a histogram of the mean values of the standard PEC estimator \hat{o}_z^{PEC} (gray) and the local PEC estimator \hat{o}_z^{LoPEC} (orange) after $m = 10^6$ samples. We obtain the histogram by generating 10^4 independent sets of m samples from the same noisy circuit. Here, $n = 65, d = 35$, and $O = Z_1$ is the Pauli Z on the first qubit. The inset plots the sites inside the light cone from O (orange dots) at different layers. We choose the circuit to be deep enough so that the light cone may cover the entire system. The figure demonstrates that both \hat{o}_z^{PEC} and \hat{o}_z^{LoPEC} are unbiased estimators of the ideal value, but the latter has a smaller variance, thus requiring much fewer samples to converge.

In Fig. 2(b), we fix the depth of the circuits ($d = 10$) and plot the sampling overhead for estimating several observables—namely Z_1, Z_1Z_{10} , and $Z_1Z_4Z_{10}$ —given circuits of different n . Here, the sampling overhead is the variance of the estimator divided by ε^2 , where $\varepsilon = 0.01$ is the desired precision. While the sampling overhead using the standard PEC estimator grows with the system size, the sampling overhead of the local PEC estimator saturates at large n .

IV. ZNE FOR LOCAL OBSERVABLES

The main idea of ZNE is to obtain expectation values at several different error rates and, from these values,

extrapolate to the zero noise limit. In contrast to PEC, ZNE is a biased estimator, and the error cannot be completely suppressed by taking more samples. In addition, the ZNE error cannot be inferred from the measurement statistics and one must rely on theoretical error bounds to guarantee the outcome is close to the ground truth. Here, we establish an error bound for ZNE that takes into account the light cone of the target observable.

In ZNE, we obtain expectation values at different error rates by amplifying the noise channels. Let $\mathcal{N}_{i,j}^{(g)}$ denote the amplified version of $\mathcal{N}_{i,j}$, constructed from $\mathcal{N}_{i,j}$ by replacing $p_{i,j}$ with $gp_{i,j}$ for some $g \geq 1$. Note that instead of amplifying $\lambda_{i,j}$ as in earlier works [3, 32], we amplify the error probability $p_{i,j}$ for simplicity. To implement such amplification with a gain factor $g \geq 1$:

$$\tilde{\mathcal{U}}^{(g)} \equiv \prod_{i=1}^d \mathcal{U}_i \prod_{j=1}^J \mathcal{N}_{i,j}^{(g)} = \prod_{i=1}^d \tilde{\mathcal{U}}_i \prod_{j=1}^J \mathcal{N}_{i,j}^{(\delta g_{i,j})}, \quad (18)$$

we probabilistically apply additional noise channels $\mathcal{N}_{i,j}^{(\delta g_{i,j})}$ with $\delta g_{i,j} = (g-1)/(1-2p_{i,j})$, before each layer of the noisy circuit. We may also perform the unitary conjugation of the noise channels through the entire circuit to obtain a convenient representation of the noisy circuit

$$\tilde{\mathcal{U}}_g = \left(\prod_{i=1}^d \prod_{j=1}^J \tilde{\mathcal{N}}_{i,j}^{(g)} \right) \mathcal{U}_d \cdots \mathcal{U}_1, \quad (19)$$

where $\tilde{\mathcal{N}}_{i,j}^{(g)}(\rho) = (1-gp_{i,j})\rho + gp_{i,j}\tilde{P}_{i,j}\rho\tilde{P}_{i,j}^\dagger$ and $\tilde{P}_{i,j} = \mathcal{U}_d \cdots \mathcal{U}_{i+1} \mathcal{U}_i(P_{i,j})$ are Pauli strings conjugated by appropriate ideal circuit layers.

With a gain factor g , we obtain the corresponding expectation value $f(g) = \text{Tr}(\tilde{\mathcal{U}}_g^\dagger(O)\rho)$, which can be represented as a polynomial function of g

$$f(g) = \sum_{k=0}^K a_k g^k + R_{K+1}(g), \quad (20)$$

where a_k are coefficients independent of g , $K \geq 1$ is a constant, and R_{K+1} is a remainder that sums over terms of higher orders in g . Note that $f(1)$ is the expectation value obtained from the bare noisy circuit and $f(0) = a_0$ is the ideal value. From the values at $g_0 = 1 < g_1 < \cdots < g_K$, one constructs a linear combination [3]

$$f_{\text{ZNE}} = \sum_{\ell=0}^K \beta_\ell f(g_\ell) = f(0) + \underbrace{\sum_{\ell=0}^K \beta_\ell R_{K+1}(g_\ell)}_{\equiv \bar{R}_{K+1}} \quad (21)$$

by demanding that $\sum_{\ell=0}^K \beta_\ell = 1$ and $\sum_{\ell=0}^K \beta_\ell g_\ell^k = 0$ for $k = 1, \dots, K$. Solving these constraints returns the coefficients β_ℓ [3]: $\beta_\ell = \prod_{m \neq \ell} [g_m / (g_\ell - g_m)]$. The linear combination in Eq. (21) gives the desired value of $f(0)$ up to a remainder that depends on high-order terms in g . Since these terms correspond to multiple-error events,

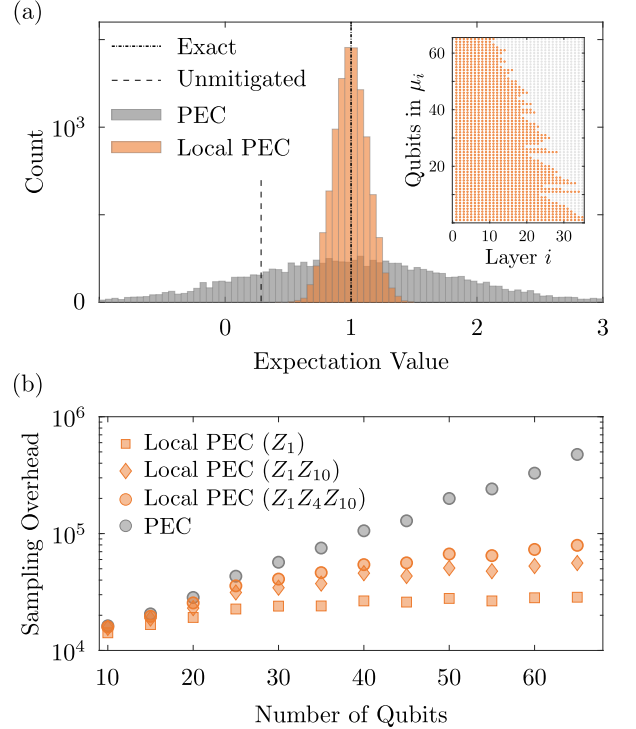


FIG. 2. Comparison between the standard PEC estimator and our local PEC estimator. (a) A histogram of expectation values obtained from 10^4 independent sets, each of 10^6 samples, using the standard PEC estimator (gray bars) and the local PEC estimator (orange bars). The inset indicates which qubits are in the light cone μ_i after layer i of the circuit. (b) The sampling overhead to achieve a fixed precision $\varepsilon = 0.01$ using the standard estimator (gray) and the local estimators (orange). The local estimators depend on the light cones of the observables, namely Z_1 (squares), Z_1Z_{10} (diamonds), and $Z_1Z_4Z_{10}$ (circles).

they should be small as long as Pauli error probabilities $p_{i,j}$ are sufficiently small.

To bound the bias in ZNE, we use Eq. (19) to expand $\text{Tr}(\rho \tilde{\mathcal{U}}_g^\dagger(O))$ in a polynomial of g_ℓ and obtain an explicit form of the remainder:

$$R_{K+1}(g_\ell) = \sum_{k=K+1}^{dJ} g_\ell^k \sum_{\nu_k} p_{\nu_k} G_{\nu_k}, \quad (22)$$

where $\nu_k = \{(i_1, j_1), \dots, (i_k, j_k)\}$ is a set of k distinct pairs (i, j) , the second sum is over all possible sets ν_k , $p_{\nu_k} \equiv p_{i_1, j_1} \cdots p_{i_k, j_k}$,

$$G_k \equiv \sum_{\sigma \in \{0,1\}^k} (-1)^{k - \text{Ham}(\sigma)} \text{Tr}(\mathcal{U}(\rho) \tilde{P}_{\nu_k}^{\sigma \dagger} O \tilde{P}_{\nu_k}^{\sigma}), \quad (23)$$

the sum in Eq. (23) is over all k -bit string σ , $\text{Ham}(\sigma)$ is the Hamming weight of σ , and $\tilde{P}_{\nu_k}^{\sigma} \equiv \tilde{P}_{i_1, j_1}^{\sigma_1} \cdots \tilde{P}_{i_k, j_k}^{\sigma_k}$ is a product of $\text{Ham}(\sigma) \leq k$ Kraus operators.

Since $|G_k| \leq 2^k$, we arrive at an upper bound for the

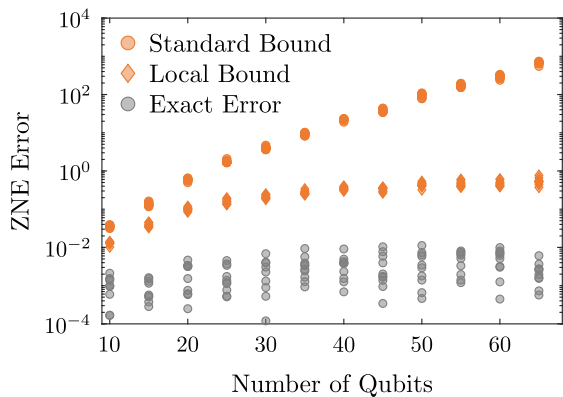


FIG. 3. A comparison between the exact ZNE error (gray circles), the standard bound [Eq. (24), orange circles], and the local bound [Eq. (26), orange diamonds] for measuring Z_1 in different randomly generated circuits. The circuits have a fixed depth of 10 and different system sizes. We applied ZNE with $K = 2$, $g_0 = 1$, $g_1 = 2$, and $g_2 = 4$. We estimated the exact error using $m = 10^6$ samples, making the shot noise negligible compared to the remainder.

remainder in Eq. (21):

$$|\bar{R}_{K+1}| \leq \sum_{k=K+1}^{dJ} 2^k \left| \sum_{\ell=0}^K \beta_{\ell} g_{\ell}^k \right| \sum_{\nu_k} p_{\nu_k}. \quad (24)$$

In practice, Eq. (24) provides a readily computable error bound for ZNE (see Appendix B for more details). To understand how this error bound scales with the error rates, we let $\Gamma_k \equiv \left| \sum_{\ell=0}^K \beta_{\ell} g_{\ell}^k \right|$, $p \equiv \max_{i,j} p_{i,j}$, $g = \max_{\ell} g_{\ell}$ and obtain a more compact bound from Eq. (24):

$$|\bar{R}_{K+1}| \leq \sum_{k=K+1}^{dJ} \Gamma_k \binom{dJ}{k} (2p)^k. \quad (25)$$

When the total experimental error rate is small, i.e. $dJgp \ll 1$, Eq. (25) implies the ZNE error is suppressed to the K th order: $|\bar{R}_{K+1}| = \mathcal{O}((2dJgp)^{K+1})$.

Both Eqs. (24) and (25) depend on the total error rate on the entire circuit. But intuitively, errors that occur outside the light cone should not contribute to the remainder in Eq. (21). In fact, we can realize this intuition in the error analysis by simply replacing $\mathcal{N}_{i,j}$ with a trivial channel if it is outside the light cone. Let $\tilde{p}_{i,j} = p_{i,j}$ if $(i,j) \in \mu$, where μ is defined after Eq. (11), and $\tilde{p}_{i,j} = 0$ otherwise. Eq. (24) can be replaced by a bound that takes into account the light cone of the observable:

$$|\bar{R}_{K+1}| \leq \sum_{k=K+1}^{dJ} 2^k \left| \sum_{\ell=0}^K \beta_{\ell} g_{\ell}^k \right| \sum_{\nu_k} \tilde{p}_{\nu_k}. \quad (26)$$

We note that, in the above bounds, we ignore shot noise and assume $f(g_{\ell})$ can be estimated exactly. In practice, we have a finite number of shots and use an estimator $\hat{f}(g)$ to estimate the expectation value at each gain factor g . The statistical error in f_{ZNE} is upper bounded by

$$\sqrt{\sum_{\ell=0}^K \frac{1}{m_{\ell}} \beta_{\ell}^2 \text{Var}[\hat{f}(g_{\ell})]} \leq \sqrt{\sum_{\ell=0}^K \frac{\beta_{\ell}^2}{m_{\ell}}}, \quad (27)$$

where m_{ℓ} is the number of shots used to estimate $f(g_{\ell})$. Combining with Eq. (26), the ZNE error is upper bounded by

$$\sqrt{\sum_{\ell=0}^K \frac{\beta_{\ell}^2}{m_{\ell}} + \sum_{k=K+1}^{dJ} 2^k \left| \sum_{\ell=0}^K \beta_{\ell} g_{\ell}^k \right| \sum_{\nu_k} \tilde{p}_{\nu_k}}. \quad (28)$$

In Fig. 3, we compare the standard error bound in Eq. (24), the local error bound in Eq. (26), and the exact error after applying ZNE with $K = 2$ and $g_0 = 1$, $g_1 = 2$, $g_2 = 4$. We randomly generate several different circuits as outlined earlier and compute the error for each of them. We use $m = 10^6$ samples for each expectation value so that the shot noise is negligible compared to the ZNE remainder. The circuits have a fixed CNOT-depth of 10 and a variable number of qubits n , from 10 to 65. Our local bound captures the behavior of the ZNE error better than the standard bound. In particular, the local bound reaches a plateau as we increase n , whereas the standard bound grows with n and becomes meaningless at large n . However, the local bound still appears to be loose by about two orders of magnitude, owing primarily to the fact that we use the worst-case bound $|G_k| \leq 2^k$. In practice, the terms in Eq. (23) typically do not add up constructively, resulting in G_k being much smaller than 2^k .

V. CONCLUSIONS

In this paper, we analyzed and improved error-mitigation techniques for measuring expectation values of local observables. Our results directly improve the performance of near-term algorithms, which heavily rely on substantial mitigation of errors in quantum devices. In particular, one can use our results and similar light-cone arguments to combine error mitigation with other techniques, including circuit knitting and classical shadow tomography.

ACKNOWLEDGMENTS

We thank Andrew Eddins, Abhinav Kandala, Youngseok Kim, Antonio Mezzacapo, Alireza Seif, and Derek Wang for helpful discussions.

-
- [1] S. Bravyi, O. Dial, J. M. Gambetta, D. Gil, and Z. Nazario, The future of quantum computing with superconducting qubits, *J. Appl. Phys.* **132**, 160902 (2022).
- [2] A. D. Córcoles, A. Kandala, A. Javadi-Abhari, D. T. McClure, A. W. Cross, K. Temme, P. D. Nation, M. Steffen, and J. M. Gambetta, Challenges and Opportunities of Near-Term Quantum Computing Systems, *Proc. IEEE* **108**, 1338 (2020).
- [3] K. Temme, S. Bravyi, and J. M. Gambetta, Error mitigation for short-depth quantum circuits, *Phys. Rev. Lett.* **119**, 180509 (2017).
- [4] Y. Li and S. C. Benjamin, Efficient Variational Quantum Simulator Incorporating Active Error Minimization, *Phys. Rev. X* **7**, 021050 (2017).
- [5] J. R. McClean, J. Romero, R. Babbush, and A. Aspuru-Guzik, The theory of variational hybrid quantum-classical algorithms, *New J. Phys.* **18**, 023023 (2016).
- [6] J. R. McClean, M. E. Kimchi-Schwartz, J. Carter, and W. A. de Jong, Hybrid quantum-classical hierarchy for mitigation of decoherence and determination of excited states, *Phys. Rev. A* **95**, 042308 (2017).
- [7] T. E. O’Brien, S. Polla, N. C. Rubin, W. J. Huggins, S. McArdle, S. Boixo, J. R. McClean, and R. Babbush, Error Mitigation via Verified Phase Estimation, *PRX Quantum* **2**, 020317 (2021).
- [8] C. Piveteau, D. Sutter, S. Bravyi, J. M. Gambetta, and K. Temme, Error Mitigation for Universal Gates on Encoded Qubits, *Phys. Rev. Lett.* **127**, 200505 (2021).
- [9] A. Kandala, K. Temme, A. D. Córcoles, A. Mezzacapo, J. M. Chow, and J. M. Gambetta, Error mitigation extends the computational reach of a noisy quantum processor, *Nature* **567**, 491 (2019).
- [10] S. Endo, S. C. Benjamin, and Y. Li, Practical Quantum Error Mitigation for Near-Future Applications, *Phys. Rev. X* **8**, 031027 (2018).
- [11] X. Bonet-Monroig, R. Sagastizabal, M. Singh, and T. E. O’Brien, Low-cost error mitigation by symmetry verification, *Phys. Rev. A* **98**, 062339 (2018).
- [12] R. Sagastizabal, X. Bonet-Monroig, M. Singh, M. A. Rol, C. C. Bultink, X. Fu, C. H. Price, V. P. Ostroukh, N. Muthusubramanian, A. Bruno, M. Beekman, N. Haider, T. E. O’Brien, and L. DiCarlo, Experimental error mitigation via symmetry verification in a variational quantum eigensolver, *Phys. Rev. A* **100**, 010302 (2019).
- [13] S. McArdle, X. Yuan, and S. Benjamin, Error-Mitigated Digital Quantum Simulation, *Phys. Rev. Lett.* **122**, 180501 (2019).
- [14] D. Su, R. Israel, K. Sharma, H. Qi, I. Dhand, and K. Brádler, Error mitigation on a near-term quantum photonic device, *Quantum* **5**, 452 (2021).
- [15] P. Czarnik, A. Arrasmith, P. J. Coles, and L. Cincio, Error mitigation with Clifford quantum-circuit data, *Quantum* **5**, 592 (2021).
- [16] W. J. Huggins, S. McArdle, T. E. O’Brien, J. Lee, N. C. Rubin, S. Boixo, K. B. Whaley, R. Babbush, and J. R. McClean, Virtual Distillation for Quantum Error Mitigation, *Phys. Rev. X* **11**, 041036 (2021).
- [17] B. Koczor, Exponential Error Suppression for Near-Term Quantum Devices, *Phys. Rev. X* **11**, 031057 (2021).
- [18] M. Cerezo, K. Sharma, A. Arrasmith, and P. J. Coles, Variational Quantum State Eigensolver, *npj Quantum Inf.* **8**, 113 (2022).
- [19] L. Cincio, K. Rudinger, M. Sarovar, and P. J. Coles, Machine Learning of Noise-Resilient Quantum Circuits, *PRX Quantum* **2**, 010324 (2021).
- [20] L. Funcke, T. Hartung, K. Jansen, S. Kühn, P. Stornati, and X. Wang, Measurement error mitigation in quantum computers through classical bit-flip correction, *Phys. Rev. A* **105**, 062404 (2022).
- [21] S. Wang, P. Czarnik, A. Arrasmith, M. Cerezo, L. Cincio, and P. J. Coles, Can Error Mitigation Improve Trainability of Noisy Variational Quantum Algorithms?, [arXiv:2109.01051](https://arxiv.org/abs/2109.01051).
- [22] E. van den Berg, S. Bravyi, J. M. Gambetta, P. Jurcevic, D. Maslov, and K. Temme, Single-shot error mitigation by coherent Pauli checks, [2212.03937](https://arxiv.org/abs/2212.03937).
- [23] R. Takagi, S. Endo, S. Minagawa, and M. Gu, Fundamental limits of quantum error mitigation, *npj Quantum Inf.* **8**, 1 (2022).
- [24] R. Takagi, H. Tajima, and M. Gu, Universal sampling lower bounds for quantum error mitigation, [arXiv:2208.09178](https://arxiv.org/abs/2208.09178).
- [25] M. C. Tran, C.-F. Chen, A. Ehrenberg, A. Y. Guo, A. Deshpande, Y. Hong, Z.-X. Gong, A. V. Gorshkov, and A. Lucas, Hierarchy of linear light cones with long-range interactions, *Phys. Rev. X* **10**, 031009 (2020).
- [26] A. M. Childs, Y. Su, M. C. Tran, N. Wiebe, and S. Zhu, Theory of Trotter Error with Commutator Scaling, *Phys. Rev. X* **11**, 011020 (2021).
- [27] C. H. Bennett, G. Brassard, S. Popescu, B. Schumacher, J. A. Smolin, and W. K. Wootters, Purification of Noisy Entanglement and Faithful Teleportation via Noisy Channels, *Phys. Rev. Lett.* **76**, 722 (1996).
- [28] E. Knill, Fault-Tolerant Postselected Quantum Computation: Threshold Analysis, [arXiv:quant-ph/0404104](https://arxiv.org/abs/quant-ph/0404104).
- [29] O. Kern, G. Alber, and D. L. Shepelyansky, Quantum error correction of coherent errors by randomization, *Eur. Phys. J. D* **32**, 153 (2005).
- [30] M. R. Geller and Z. Zhou, Efficient error models for fault-tolerant architectures and the Pauli twirling approximation, *Phys. Rev. A* **88**, 012314 (2013).
- [31] J. J. Wallman and J. Emerson, Noise tailoring for scalable quantum computation via randomized compiling, *Phys. Rev. A* **94**, 052325 (2016).
- [32] E. van den Berg, Z. K. Mineev, A. Kandala, and K. Temme, Probabilistic error cancellation with sparse Pauli-Lindblad models on noisy quantum processors, [arXiv:2201.09866](https://arxiv.org/abs/2201.09866).

Appendix for “Locality and Error Mitigation of Quantum Circuits”

In this Appendix, we provide additional mathematical details on the local PEC estimator and on the ZNE error bound. In Appendix A, we derive the mean of the local PEC estimator [Eq. (13)]. In Appendix B, we discuss the classical computation of the upper bound on the ZNE remainder. In Appendix C, we provide detailed specifications for the numerics presented in the main text.

Appendix A: Mean and variance of the local PEC estimator

In this section, we prove the claim in Eq. (13) that the mean of $\hat{\delta}_z^{\text{LoPEC}}$ is the ideal expectation value of the observable. We start with the definition:

$$\mathbb{E}_\sigma \mathbb{E}_z [\hat{\delta}_z^{\text{LoPEC}}] = \sum_\sigma \sum_z \prod_{(i,j) \in \mu} \gamma_{i,j} \sigma_{i,j} O_z p(\sigma_{i,j}) p(z) \quad (\text{A1})$$

$$= \sum_\sigma \sum_z \prod_{(i,j) \in \mu} \gamma_{i,j} \sigma_{i,j} O_z p(\sigma_{i,j}) \text{Tr} \left(\prod_{i'=1}^d \tilde{\mathcal{U}}_{i'} \prod_{j'=1}^J \mathcal{P}_{i',j'}^{\sigma_{i',j'}}(\rho) |z\rangle\langle z| \right) \quad (\text{A2})$$

$$= \sum_\sigma \prod_{(i,j) \in \mu} \gamma_{i,j} \sigma_{i,j} p(\sigma_{i,j}) \text{Tr} \left(\prod_{i'=1}^d \tilde{\mathcal{U}}_{i'} \prod_{j'=1}^J \mathcal{P}_{i',j'}^{\sigma_{i',j'}}(\rho) O \right) \quad (\text{A3})$$

$$= \sum_\sigma \prod_{(i,j) \in \mu} \gamma_{i,j} \sigma_{i,j} p(\sigma_{i,j}) \text{Tr} \left(\rho \prod_{i'=d}^1 \prod_{j'=1}^J \mathcal{P}_{i',j'}^{\sigma_{i',j'}} \tilde{\mathcal{U}}_{i'}^\dagger(O) \right), \quad (\text{A4})$$

where $p(\sigma_{i,j}) = 1 - p_{i,j}$ if $\sigma_{i,j} = 1$ and $p(\sigma_{i,j}) = p_{i,j}$ otherwise. By construction, we have

$$\sum_{\sigma_{i,j} = \pm 1} \gamma_{i,j} \sigma_{i,j} p(\sigma_{i,j}) \mathcal{P}_{i,j}^{\sigma_{i,j}} = \mathcal{N}_{i,j}^{-1}, \quad (\text{A5})$$

$$\sum_{\sigma_{i,j} = \pm 1} p(\sigma_{i,j}) \mathcal{P}_{i,j}^{\sigma_{i,j}} = \mathcal{N}_{i,j}. \quad (\text{A6})$$

Therefore

$$\mathbb{E}_\sigma \mathbb{E}_z [\hat{\delta}_z^{\text{LoPEC}}] = \text{Tr} \left(\rho \prod_{i=d}^1 \left(\prod_{j:(i,j) \in \mu} \mathcal{N}_{i,j}^{-1} \right) \left(\prod_{j:(i,k) \notin \mu} \mathcal{N}_{i,j} \right) \prod_{j=1}^J \mathcal{N}_{i,j} \mathcal{U}_i^\dagger(O) \right). \quad (\text{A7})$$

For the pairs (i, j) inside the light cone, $\mathcal{N}_{i,j}^{-1}$ cancels $\mathcal{N}_{i,j}$:

$$\mathbb{E}_\sigma \mathbb{E}_z [\hat{\delta}_z^{\text{LoPEC}}] = \text{Tr} \left(\rho \prod_{i=d}^1 \left(\prod_{j:(i,j) \notin V} \mathcal{N}_{i,j}^2 \right) \mathcal{U}_i^\dagger(O) \right). \quad (\text{A8})$$

Since we are left with only noise channels outside the light cone, we can replace them with the identity channel to obtain

$$\mathbb{E}_\sigma \mathbb{E}_z [\hat{\delta}_z^{\text{LoPEC}}] = \text{Tr} \left(\rho \prod_{i=d}^1 \mathcal{U}_i^\dagger(O) \right) = \langle \mathcal{U}^\dagger(O) \rangle. \quad (\text{A9})$$

This completes the proof of Eq. (14).

Appendix B: Computing the bounds on the ZNE remainder

In this section, we discuss some practical details on classically computing the bounds in Eq. (24) and, similarly, Eq. (26). For large values of dJ , looping over $k = K + 1, \dots, dJ$ and computing $\binom{dJ}{k}$ values of p_{ν_k} appear to be inefficient. Instead, we compute the bound using the following lemma:

Lemma 1. For all $k \geq K + 1$,

$$\text{sign} \left(\sum_{\ell=0}^K \beta_{\ell} g_{\ell}^k \right) = (-1)^K. \quad (\text{B1})$$

Proof. Let $h(x) \equiv \sum_{\ell=0}^K \beta_{\ell} g_{\ell}^x$ be a continuous function of $x \in \mathbb{R}$. The function $h(x)$ is an exponential polynomial that has at most K zeros. Recall that $h(1) = h(2) = \dots = h(K) = 0$, so its K zeros are exactly at $x = 1, \dots, K$. Therefore, $h(x)$ never changes the sign for all $x > K$. Since $h(0) = 1$ is positive and $h(x)$ changes its sign whenever x increases past a zero, it follows that $\text{sign}(h(x)) = (-1)^K$ for all $x > K$. \square

Using Lemma 1, we can remove the absolute value in Eq. (24) to obtain

$$\begin{aligned} |\bar{R}_{K+1}| &\leq (-1)^{K+1} \sum_{k=K+1}^{dJ} 2^k \sum_{\ell=0}^K \beta_{\ell} g_{\ell}^k \sum_{\nu_k} p_{\nu_k} \\ &= (-1)^{K+1} \sum_{\ell=0}^K \beta_{\ell} \left[\prod_{i=1}^d \prod_{j=1}^J (1 + 2g_{\ell} p_{i,j}) - \sum_{k=0}^K 2^k g_{\ell}^k \sum_{\nu_k} p_{\nu_k} \right]. \end{aligned} \quad (\text{B2})$$

In the last line, we add and subtract the sum over $k = 0, \dots, K$ and use the binomial expansion to rewrite the sum over $k = 0, \dots, dJ$. For a small K , both terms in Eq. (B2) can be computed efficiently.

Appendix C: Specifications for the numerical examples

In this section, we provide detailed specifications for the numerics presented in the main text. In all of our examples, we assume a system of qubits with the same connectivities as that of IBM's Ithaca device, which hosts 65 qubits in a heavy hex lattice Fig. 4(a). In examples where the number of qubits n are fewer than 65, we use the first n qubits according to the labels in Fig. 4(a).

In our examples, we benchmark the error mitigation strategies on circuits composing of layers of CNOTs and random single-qubit Clifford gates Fig. 4(b). The CNOT layers alternate between the three presets described in Fig. 4(b). Every three CNOT layers is followed by a layer consisting of random single-qubit gates uniformly and independently chosen from $\{H, S\}$, where

$$H = \frac{1}{\sqrt{2}} \begin{pmatrix} 1 & 1 \\ 1 & -1 \end{pmatrix}, \quad S = \begin{pmatrix} 1 & 0 \\ 0 & i \end{pmatrix}. \quad (\text{C1})$$

Additionally, each CNOT layer is preceded by $J = 10n$ randomly generated noise channels

$$\mathcal{N}_{i,j}(\rho) = e^{\mathcal{L}^{i,j}} \rho = (1 - p_{i,j})\rho + p_{i,j} P_{i,j} \rho P_{i,j}^{\dagger}. \quad (\text{C2})$$

For a given CNOT layer i , we generate a random sparse matrix $C_i \in \{0, 1, 2, 3\}^{J \times n}$ so that its j th row specifies a Pauli string $P_{i,j}$, with the convention that $0 \rightarrow \mathbb{I}, 1 \rightarrow X, 2 \rightarrow Y$, and $3 \rightarrow Z$. We choose the density of C_i —the fraction of nonzero entries in C_i —so that the average weight of $P_{i,j}$ is two. We then choose each $p_{i,j}$ uniformly random between 0 and 8×10^{-4} so that the average error rate per CNOT gate is 4×10^{-3} (there are, on average, 10 error channels per CNOT gate).

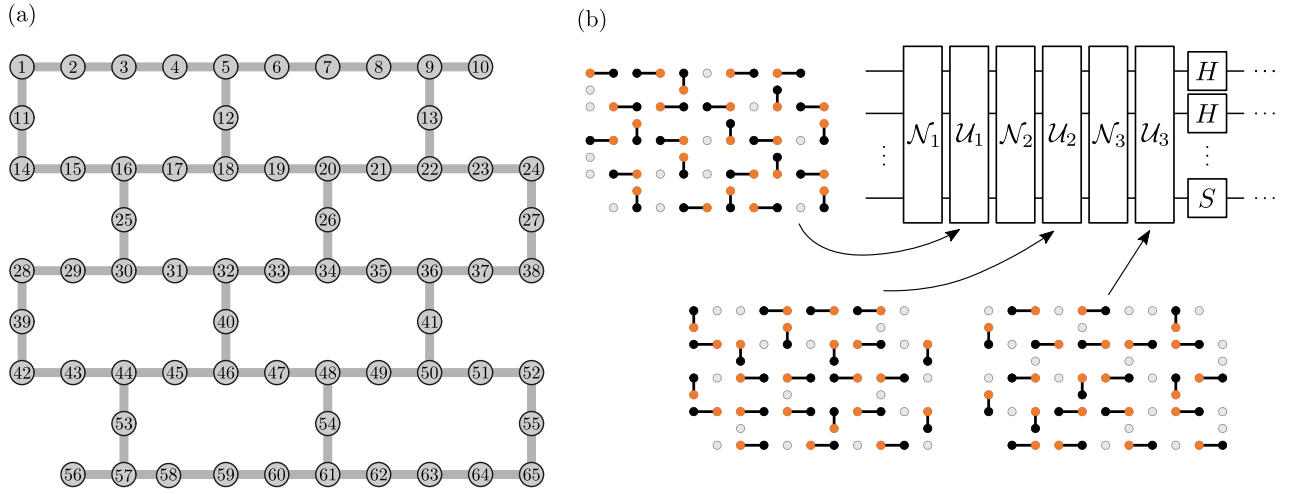


FIG. 4. An illustration of the systems and the circuits considered in our examples. (a) The connectivities (gray lines) between 65 qubits (gray circles) of IBM’s Ithaca device. In our examples, systems of $n < 65$ qubits will consist of the first n qubits ordered by the labels indicated above. (b) The circuits in our examples consist of CNOT layers and single-qubit gates. The CNOT layers alternate between three depicted presets, where a black line indicates a CNOT gate with the black qubit being the control and the orange qubit being the target. The single-qubit gates are chosen randomly between H and S .